MNRAS **000**, 000–000 (0000) Preprint 30 March 2018 Compiled using MNRAS LATEX style file v3.0

Lyman-α photons through rotating outflows

Maria Camila Remolina-Gutiérrez[1] ⋆ & Jaime E. Forero-Romero [1] †
[1] *Departamento de Física, Universidad de los Andes, Cra. 1 No. 18A-10 Edificio Ip, CP 111711, Bogotá, Colombia*

30 March 2018

ABSTRACT
Outflows and rotation are two ubiquitous kinematic features in the gas kinematics of galaxies. Here we perform Monte Carlo radiative transfer simulations of outflowing gas with additional solid body rotation to understand how these kinematic features impact the morphology of the Lyman-α emission line. We explore a range of Hydrogen optical depth of $10^5 \leq \tau_{\rm H} \leq 10^7$, rotational velocity $0 \leq v_{\rm rot}/{\rm km\ s^{-1}} \leq 100$ and outflow velocity $0 \leq v_{\rm out}/{\rm km\ s^{-1}} \leq 50$. We find three important consequences of rotation. First, it introduces a dependency with viewing angle; second it produces a line broadening and third it increases the flux at the line's center. We also develp a semi-analytic model that modifies the spectra of pure outflow simulations that manages to reproduce the line widths and flux change at the line's center within a 7% and 50% precision, respectively.

Key words: galaxies: dwarf — radiative transfer — Methods: numerical

1 INTRODUCTION

The interpretation of the Lyman-α emission in galaxies is key to understand their evolutionary processes, specially in star-forming, low-dust galaxies (Partridge & Peebles 1967). Recent improvements in instrumentation have revolutionized the kind of studies that can be performed on Lyman-α emitting galaxies (LAEs.) For instance, it is now possible to infer detailed kinematic maps for nearby galaxies. The study of these maps would allow us to build data-driven models to interpret the Lyα spectra of unresolved galaxies, helping us to constrain the physical conditions of the interstellar medium (ISM) processing the Lyα radiation.

For instances, dwarf galaxies show signs of coherent rotation (Swaters et al. 2009). Some of them are expected to have high neutral gas contents and thus show Lyα emission with rotation imprints (**???**) Some Compact Dwarf Galaxies actually show gas kinematics that range from pure rotation to high velocity dispersion without a clear rotation pattern. (Cairós et al. 2015; Cairós & González-Pérez 2017)

The case for outflows as traced in the Lyα line is much better stablished. In many cases the Lyα line profiles has a single peak redwards from the line's center, in other cases there is a double peak but the peak on the red side is stronger (e.g. **???**). These features been readily explained as the consequence of multiple Lyα photon scatterings through an homogeneous outflowing shell of neutral Hydrogen (**?**Orsi et al. 2012; **?**; **?**).

Here we present for the first time a study of the joint effects of galaxy outflows and rotation, two of the three major kinematic components expected in LAEs. We study a simplified geometrical configuration corresponding to a spherical gas cloud with symmetrical radial outflows and a rotation profile corresponding to a solid body. We base our modeling on a Monte-Carlo radiative transfer code called CLARA (Code for Lyman Alpha Radiation Analysis) presented for the first time by Forero-Romero et al. (2011).

Besides modeling the impact of joint rotation and outflows, we also check to what extent the analytical model presented by Garavito-Camargo et al. (2014) to explain the effects of rotation can also be applied in our case. We show how solid body rotation effects can be modelled by postprocessing the results of outflow only simulation.

in the results of other radiative transfer model in the case of large optical depths. In this case it is a good approximation to Doppler boost the results of the model without rotation.

The structure of the paper is the following. We introduce first our theoretical tools and assumptions in Section 2. We continue in Section 3 with the results from the Monte-Carlo simulation, the comparison against the semi-analytical approximation which we use to make a thorough exploration of the effect of rotation. In Section 4 we discuss our results and their possible implications for observational analysis to finally present our conclusions in Section 5.

⋆ mc.remolina197@uniandes.edu.co
† je.forero@uniandes.edu.co

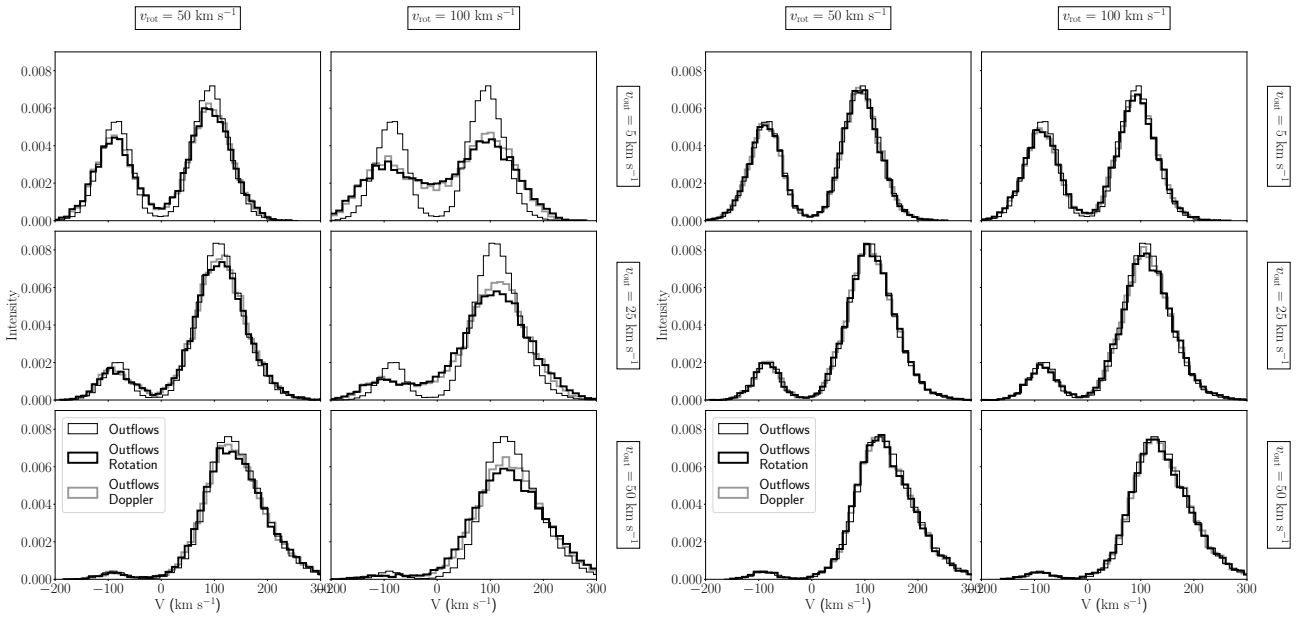

Figure 1. Qualitative trends of changing outflow and rotational velocity viewed perpendicular/paralell to the rotation axis. Here we fix $\tau_{\rm H} = 10^6$. The six panels on the left correspond to $\theta = 90°$ and the panels on the right to $\theta = 0°$ We vary $v_{\rm rot}$ increasing from left to right and $v_{\rm out}$ increasing from top to bottom. The thin black line corresponds to the Lyα line obtained with CLARA without any rotation and the indicated outflow velocity. The thick black line corresponds to the results including both outflows and rotation. The thick gray line shows the results of modifyin the pure outflow solution by the Doppler shift presented in Equation 4 (in thin line), if there is a radiative transfer of rotation and outflows (thick and clear line), and if there is a radiative transfer of only outflows, but also a Doppler shift from the rotational velocity (thick and dark line).

2 THEORETICAL MODELS

The Monte Carlo code we use (CLARA) follows the propagation of individual photons through a neutral Hydrogen medium characterized by its temperature, velocity field and global optical depth. The code assumes an homogeneous density throughout the simulated volume. In the current implementation we neglect the influence of dust. Our basic model is an spherical distribution of neutral hydrogen, an approximation commonly used in the literature, as it explains a wide variety of observational features (Ahn et al. 2003; Verhamme et al. 2006; Dijkstra et al. 2006).

The velocity field we use captures both outflows and rotation. Outflows are described by a Hubble-like radial velocity profile with the velocity magnitude increasing linearly with the radial coordinate; the outflows model is fully characterized by $v_{\rm out}$, the velocity at the sphere's surface. Rotation follows a solid body rotation profile, which is fully characterized by $V_{\rm rot}$, the linear velocity at the sphere's surface.

The total velocity field corresponds to the superposition of rotation and outflows. The cartesian components take the following form:

$$v_x = \frac{x}{R} V_{\rm out} - \frac{y}{R} V_{\rm rot}, \quad (1)$$

$$v_y = \frac{y}{R} V_{\rm out} + \frac{x}{R} V_{\rm rot}, \quad (2)$$

$$v_z = \frac{z}{R} V_{\rm out}, \quad (3)$$

where x, y and z are the cartesian position coordinates with the origin at the sphere's center, R is the radius of the sphere and the direction of the angular velocity vector corresponds to the $\hat{k}$ unit vector.

For each model setup we follow 10^5 individual photons generated at the center of the sphere at the Lyα line's center as they propagate through the volume and finally scape. We store the final frequency and propagation direction for each photon at its last scattering.

In Table **??** we list the combination of $\tau_{\rm H}$, $v_{\rm rot}$ and $v_{\rm rot}$ values used in this paper. The range of values have some overlap with the expectations from a galaxy with a total neutral hydrogen mass of 10^8-10^9 $M_\odot$. We run a total of 27 different models.

Garavito-Camargo et al. (2014) presented an analytical model that accounts for the effects of pure rotation on the Lyα line morphology. The basic assumption of their analytical model is that each differential surface element on the sphere Doppler shifts the photons that it emits. In this paper we introduce this ansatz by post-processing the results of the outflows simulations without rotation. The frequency of each photon is Doppler shifted as follows

$$x' = x + \frac{\vec{V}_{\rm rot} \cdot \hat{k}}{v_{\rm th}} \quad (4)$$

where x' is the photon's new frequency, x is the photon's frequency after being procesed by the outflow, $v_{\rm rot}$ is the rotational velocity at the point of escape of the photon, $\hat{k}$ is the photon's direction of propagation and $v_{\rm th}$ is the thermal velocity of the sphere.

This allows us to produce new Lyα spectra and compare

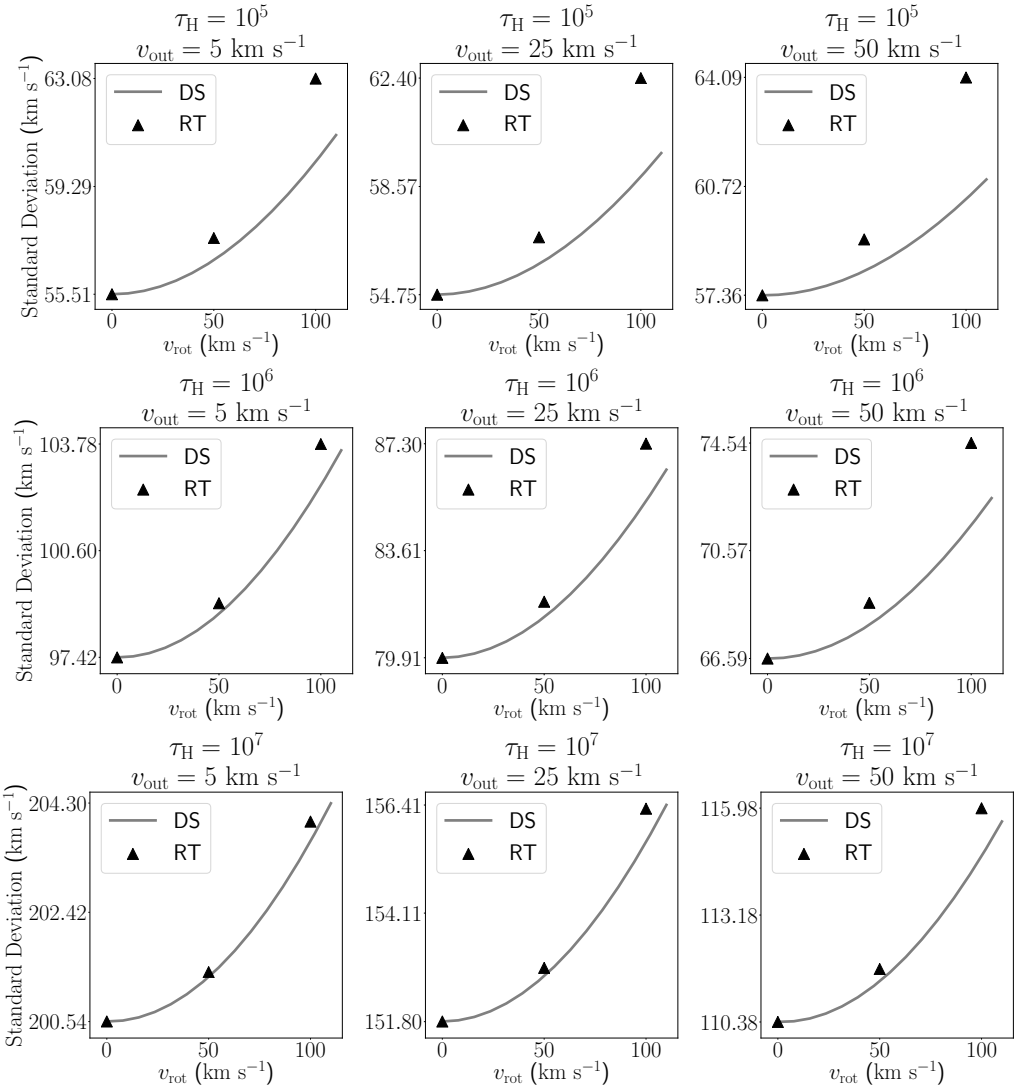

Figure 2. Standard Deviation trends. Results for all the Radiative Transfer simulations (in triangles) compares against the Doppler Shift model (lines). All panels correspond to a viewing angle of $\theta = 90°$ (perpendicular to the rotation axis). The optical depth increases from top to bottom and the outflow velocity from left to right.

them with the full radiative transfer solution including both outflows and rotation.

3 RESULTS

3.1 Qualitative Trends

Figure 1 summarizes the most important trends. The six panels correspond to $\tau = 10^6$ and a viewing angle of $\theta = 90°$, that is, perpendicular to the rotation axis of the galaxy. In every panel the thin black line corresponds to the pure outflow solution, i.e. without rotation. From top to bottom we see the effect of increasing the outflow velocity, which is the expected increasing asymmetry towards the red peak.

The thick black line corresponds to the solution that includes both outflows and rotation. Comparing the left and right columns (lower versus higher rotational velocity) we can see two immediate effects. First, the line broadens and second, the intensity at the line's center increases.

The thick gray line correspods to the pure outflow solution with the Doppler boost added to model rotation's influence. At $\tau_H = 10^6$ the Doppler boost does a good job at capturing the broad morphological features introduced by rotation: the angle dependence, the broadening and the intensity increase at the line's center.

In Figure **??** we show the same results as in Figure 1 but for a viewing angle of $\theta = 90°$, that is parallel to the rotation axis. In this case we confirmethe result presented by Garavito-Camargo et al. (2014), namely that pure rotation introduces a strong dependence with viewing angle, a trend that we find also holds for rotation mixed with ouflows.

The quality of the results from the Doppler boost improves for higher τ_H values. In the Appendix we show the same plots as Figures 1 and 1, there it is evident that for $\tau_H = 10^5$ the results are not as good as they are for $\tau_H = 10^6$,

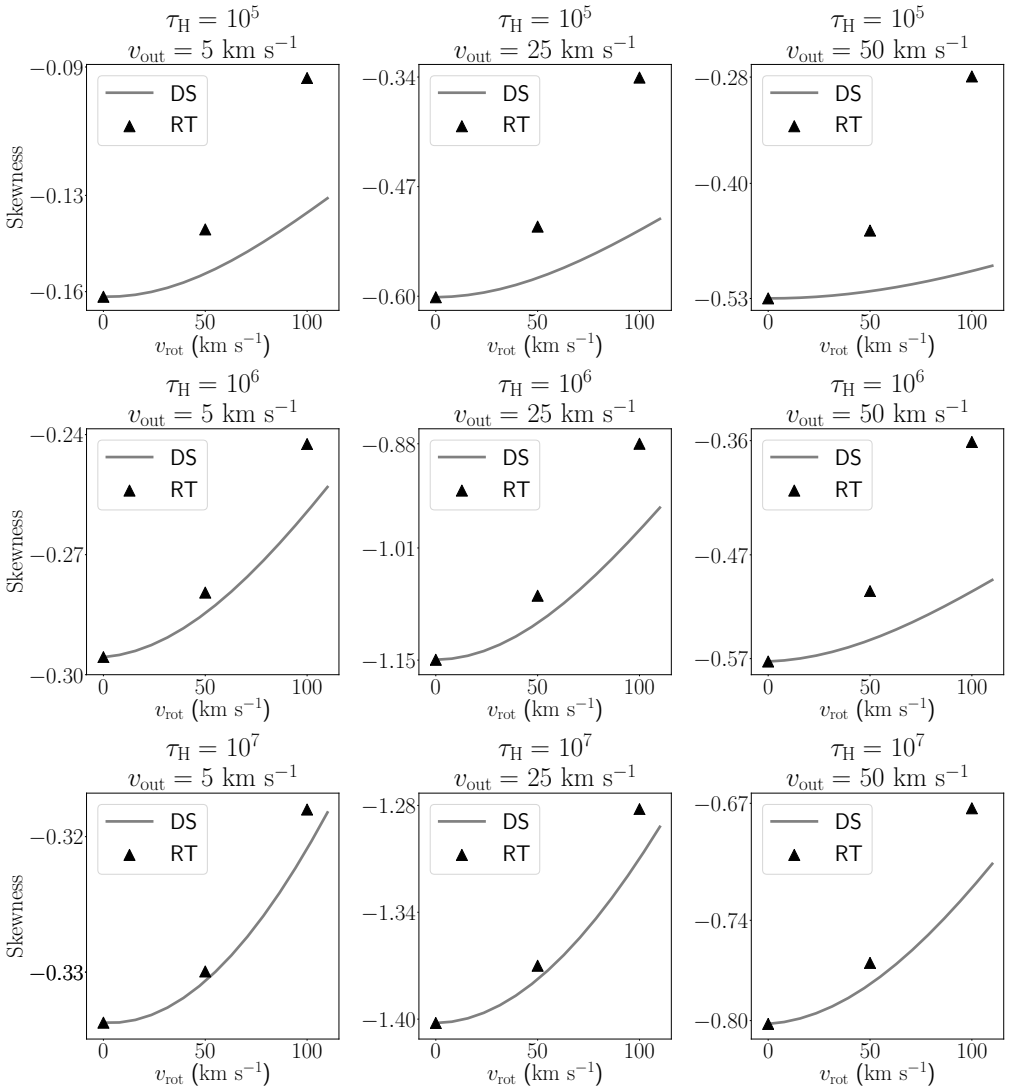

Figure 3. Skewness trends. Results for all the Radiative Transfer simulations (in triangles) compares against the Doppler Shift model (lines). Follows the same layout as Figure 2.

and that for $\tau_H = 10^7$ the Doppler boos provides a remarkable good approximation.

3.2 Quantitative trends

After finding the quantitative influence of the different parameters we move onto a qualitative study. To do this we summarize the line morphology by four different characteristics: standard deviation (STD), skewness (SKW), bimodality (BI) and valley/peak ration. These quantities are defined by the following equations (Kokoska & Zwillinger 1999).:

$$\mathrm{STD} = \sqrt{m_2}, \tag{5}$$

$$\mathrm{SKW} = \frac{m_3}{m_2^{3/2}}, \tag{6}$$

$$\mathrm{BI} = \mathrm{KURTOSIS} - \mathrm{SKW}^2 = \frac{m_4}{m_2^2} - \frac{m_3^2}{m_2^3}, \tag{7}$$

where each m_i is the i-th moment about the mean. The STD has velocity units and quantifies the line's width. The SKW is adimensional and quantifies the peaks' asymmetry. In the case of a bimodal distribution, $SKW > 0$ means that the blue peak is taller and for $SWK < 0$ the red peak is taller. The BI is adimensional and quantifies whether the line has 1 or 2 peaks: it is always ≥ 1 (Pearson 1929) and the to 1, the more bimodal is the line (i.e. has 2 similar peaks). We found by visual inspection of our spectra that BI= 2.5 marks the transition between two peaks (however imbalanced) and a dominang single peak.

3.2.1 Standard Deviation

Figure 2 summarizes the standard deviation results for all our models. Each panel shows the STD as a function of v_{rot} . All panels were computed using a viewing angle of $\theta = 90°$ (perpendicular to the rotation axis), which has the most extreme ifluence from rotation. The black triangles correspond

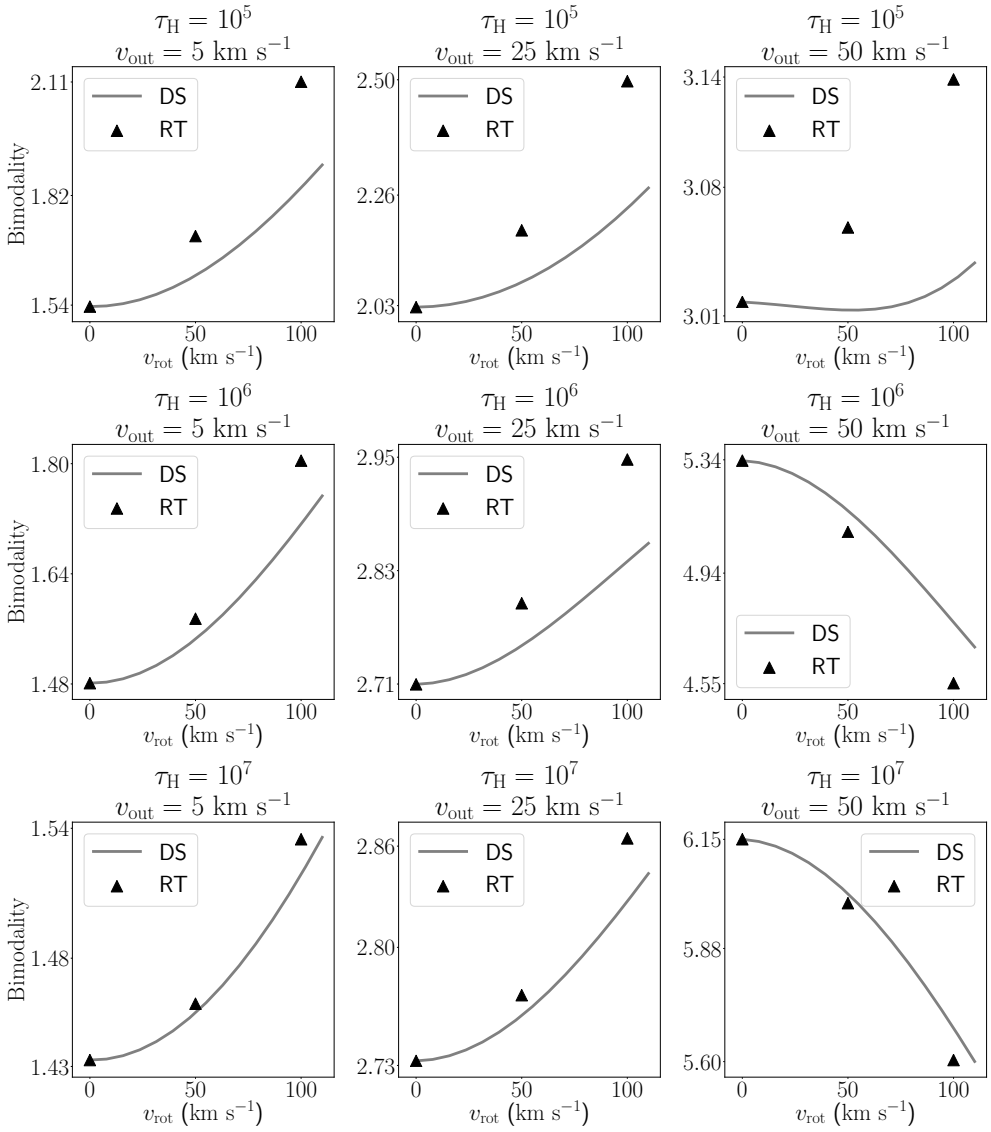

Figure 4. Bimodality trends. Results for all the Radiative Transfer simulations (in triangles) compares against the Doppler Shift model (lines). Follows the same layout as Figure 2.

to the full RT solution and the line to the DS approximation. The optical depth increases from top to bottom and the outflow velocity from left to right. This quantitative plot confirms that the line width increases with rotational velocity and optical depth. These trends are expected; higher rotational velocities can be seen as an addition of different Doppler shifts that smear out the line, while a higher optical depth translates into a larger number of scatterings that increase the probability of a photon to diffuse in frequency resulting in a broader line.

The DS successfuly reproduces all trends with the optical depth, rotational velocity and outflow velocity. However, the DS consistently underestimates the STD. The difference between the RT and DS increases with the outflow velocity and the rotational velocity, and decreases with increasing optical depth. In the range of parameter space explore, this difference has as an upper bound of $\sim 7\%$, 3% and $\sim 2\%$ for $\tau_H = 10^5$, 10^6 and 10^7, respectively.

3.2.2 Skewness

Figure 3 presents the skwewness results for all the models together with the DS comparison following the same layout as Figure 2. In all cases the skewness is negative showing that all the lines are unbalanced towards the red side of the spectrum. Skewness increases with rotational velocity and decreases with optical depth; rotation tries to smoothes the line diminishing the asymetries while a higher optical depth reinforces the line asymetries. The skewness does not have a monotonous trend with outflow velocity because there is a transition between double and single peak line; for low outflow velocities the skewness signals the balance between the two existing peaks while for high outflow velocities it quantifies the asymmetry of the already dominant read peak.

The DS reproduces the main trends, again with an underestimation that decreases at higher optical depths and increases with larger values of the rotational velocity and

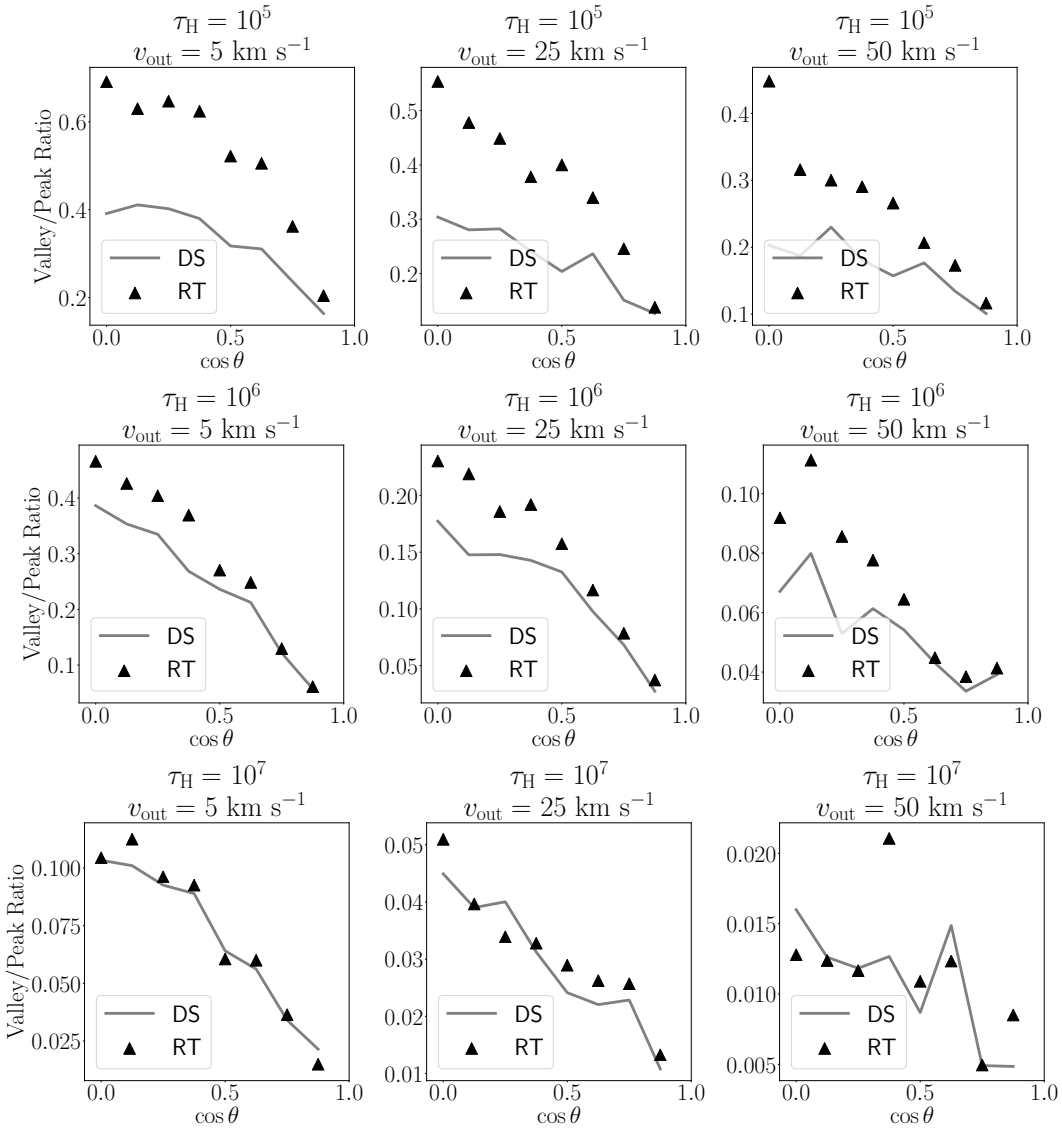

Figure 5. Valley Intensity: We show for each τ_H the dependency that the viewing angle θ has on the line's the valley intensity. The larger $\cos\theta$ the lower is the valley intensity, so the higher θ, the higher the valley intensity. Also, the higher τ_H , the better is the fit RT-DS. We fixed $v_{rot} = 100$km s^{-1}.

outflow velocity. In this case the differences between RT and DS have an upper bound of 85%, 35% and 5% for $\tau_H = 10^5$, 10^6 and 10^7, respectively.

3.2.3 Bimodality

Figure 4 shows the results for the bimodality using the same layout as in the two previous Figures. Following the reasoning about the skewness, we observe that increasing the outflow velocity increases the value of bimodality, that is, it transitions to a more pronounced single peak. The trend as a function of the rotational velocity and the optical depth are not monotonous. When the outflow velocity is low ($v_{out} < 50$ km s^{-1}), an increasing rotational velocity smears the two asymmetrical peaks pushing the line morphology towards a single peaks, making the bimodality statistics increase. On other situations ($v_{out} = 50$ km s^{-1} and $\tau_H \geq 10^6$) higher rotational velocities the bimodality statistics decreases, which means that it manages to slightly enlarge the already dominant red peak.

The DS reproduces the main trends while underestimating the bimodality statistics. As expected from the previous results the difference betwen RT and DS decreases at higher optical depths and increases with increasing values of the rotational and outflow velocities. In this case the differences have an upper bound of 4%, 2% and 1% for $\tau_H = 10^5$, 10^6 and 10^7, respectively.

3.2.4 Intensity at line's center

In Figure 5 we quantify how the intensity at the line's center (i.e. the valley) changes with the viewing angle, the outflow velocity and the optical depth. These results correspond to a fixed rotational velocity of $v_{rot} = 100$ km s^{-1}. The triangles

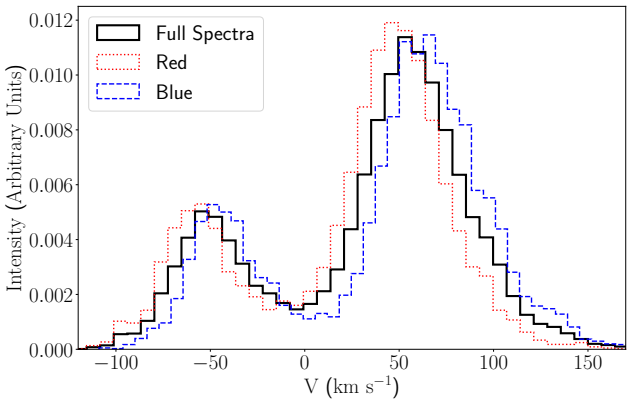

Figure 6. Spectra from receeding/approaching sides of a toy model LAE. These results correspond to the RT simulation with $v_{\rm out} = 25$km s^{-1}, $v_{\rm rot} = 50$km s^{-1}, $\tau_{\rm H} = 10^5$. The spectra were computed for a viewing angle of $\theta = 90°$.

correspond to the RT simulations and the line represents the DS results. The valley intensity is expresed as a fraction of the maximum peak intensty in the line, as such the valley/peak ratio is always less than one. In every panel we see that the valley/peak ratio decreases as the observer moves from a line of sight perpendicular to the rotation axis onto a parallel line of sight. This is a clear demonstration of the viewing angle dependency introduced by rotation.

The valley/peak ratio at $\cos\theta = 1$ matches results without rotation, this shows that for increasing rotational velocity the valley/peak ratio increases. In turn, for increasing optical depth or outflowing velocity this ratio decreases. Once again, the DS results correctly follow the trends for the full RT simulations. This time the differences have an upper bound of 55%, 2% and 1% for $\tau_{\rm H} = 10^5$, 10^6 and 10^7, respectively.

4 DISCUSSION

4.1 Theoretical Insights

A first approach to an analytical expression that returns the Lyα spectrum from a rotating galaxy is presented by Garavito-Camargo et al. (2014). This derivation is based on the assumption that the distribution of photons' propagation directions at the edge of the galaxy is anisotropic and depends of $\tau_{\rm H}$ only. So this approximation becomes more accurate with higher optical depth and it is also the reason why the Doppler Shift technique to induce rotational effects to an outflow Lyα spectrum works.

4.2 Links to observations

There are at least three inmmediate ways the work we have presented here can be useful to observational efforts.

4.2.1 Lyα Kinematic Maps

The first is related to the capability of spatially resolving the extent of a LAE. For instance Prescott et al. (2015) presented observational results of a Doppler shift when taking spectra at two oposite sides of a LAE.

In Figure 6 we present a toy model ($v_{\rm rot} = 50$ km s^{-1}, $v_{\rm out} = 25$ km s^{-1} and $\tau_{\rm H} = 10^5$) for the spectrum of a LAE taken from to different sides of the galaxy. As the LAE is rotating, one side is being redshifted while the other is blueshifted. We see that the full spectrum is a weighted line, in solid black, that is found between these two. We notice that the distance between the maxima of the blue and red spectra is not twice the rotational velocity as it could be naively expected.

Although it is a good approximation to think the rotating spectra by a sum of Doppler shifts, the peak of the spectra is also weighted by the amount of mass with a given velocity. In this toy model the distance between the peaks of the receeding/approaching spectra is close to ~ 20 km s^{-1}, which is less than half of the naively expected value of $2v_{\rm rot} = 100$ km s^{-1}, due to the fact that only a small fraction of the photons are emitted at the extreme of the galaxy having the maximum rotational velocity of 50 km s^{-1}.

New spectrographs like MUSE should help obtain kinematic information from LAEs to build velocity maps in Lyα . This could be a natural extension of the work reported by Herenz et al. (2016) on the velocity maps of several LARS (Lyman Alpha Reference Sample) galaxies. The interpretation of such data should take into account the insights and trends we have presented in this paper.

4.2.2 Lyα continuum escaping or rotation?

Another application of this new model to the current interpretation of Lyα spectra, is that the central ($V = 0$) emission of the spectra seen in the Lyα line, is a consequence of the viewing angle of the galaxy and can be controlled by it. Several authors have suggested that this central emission is caused by radiation that escapes the galaxy without scattering. Rotation is an alternative that solves this issue.

We note that the relative intensity of the two peaks in the outflowing spectra is not modified by rotation, that asymmetry is solely controled by the outflow velocity. This means that results that have already derive a typical outflowing velocity as to match the observational constraints do not have to be completely revised. Only an additional exploration of rotational velocities and viewing angles need to be explored.

5 CONCLUSIONS

In this paper we explore, for the first time in the literature, the results of a model for the emergent Lyα line from rotating outflows. The main results for the model are computed from a Monte-Carlo radiative transfer simulation and confronted with a simple semi-analytic ansatz that adds the effects of rotation onto results of pure outflow kinematics.

The main effects of rotation on the Lyα line morphology are:

- Broadening the line.
- Increasing the intensity at the line's center.
- Inducing a dependency on the viewing angle, The closer

the observer is to the pole of the galaxy (defined by the rotation axis), the smaller are the effects from rotation.

We found that in the case of solid body rotation these effects can be quantitatively explained by a Doppler boost, where the Doppler factor can be computed as the producet of quantities at the surface of last scattering, namely $\vec{v}_{\rm rot} \cdot \hat{k}$, where $\vec{v}_{\rm rot}$ is the velocity due to rotation and $\hat{k}$ is the direction of the photon's propagation. These conclusions, specially the confirmation of the Doppler boost as a good proxy for solid body rotation, strenghten the evidence reported by Garavito-Camargo et al. (2014) when they modeled the effect of pure rotation on Lyα spectra.

As an application to observational data we find that recent results that take the spectra of two different sides of a galaxy can detect the effect of approaching/receeding gas motions. However, the distances between the peaks of these two spectra correspond to $\approx v_{\rm rot} \cos\theta$ due to the weights of the emitting regions.

REFERENCES

Ahn S.-H., Lee H.-W., Lee H. M., 2003, MNRAS, 340, 863
Cairós L. M., González-Pérez J. N., 2017, A&A, 600, A125
Cairós L. M., Caon N., Weilbacher P. M., 2015, A&A, 577, A21
Dijkstra M., Haiman Z., Spaans M., 2006, ApJ, 649, 14
Forero-Romero J. E., Yepes G., Gottlöber S., Knollmann S. R., Cuesta A. J., Prada F., 2011, MNRAS, 415, 3666
Garavito-Camargo J. N., Forero-Romero J. E., Dijkstra M., 2014, ApJ, 795, 120
Herenz E. C., et al., 2016, A&A, 587, A78
Kokoska S., Zwillinger D., 1999, CRC standard probability and statistics tables and formulae. Crc Press
Orsi A., Lacey C. G., Baugh C. M., 2012, MNRAS, 425, 87
Partridge R. B., Peebles P. J. E., 1967, ApJ, 147, 868
Pearson K., 1929, Biometrika, 21, 370
Prescott M. K. M., Martin C. L., Dey A., 2015, ApJ, 799, 62
Swaters R. A., Sancisi R., van Albada T. S., van der Hulst J. M., 2009, A&A, 493, 871
Verhamme A., Schaerer D., Maselli A., 2006, A&A, 460, 397

APPENDIX A: ADDITIONAL FIGURES

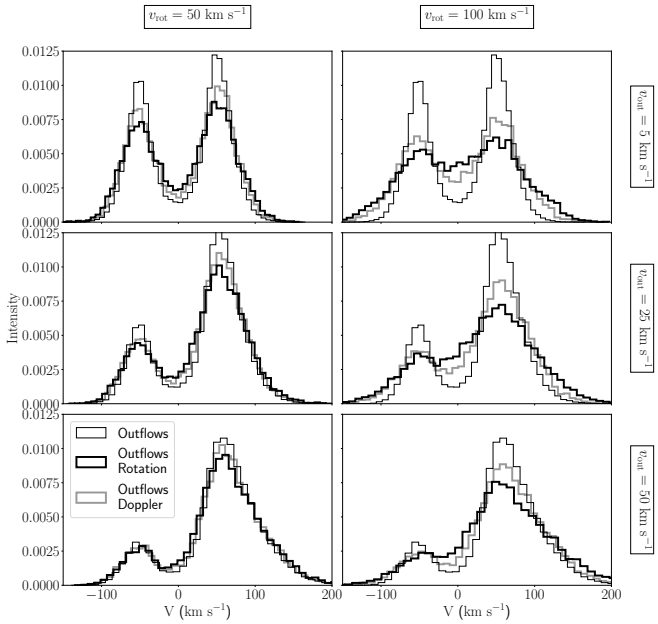

Figure A1. Qualitative trends of changing outflow and rotational velocity. Same layout as Figure 1, this time $\tau_{\rm H} = 10^5$ and $\theta = 90°$.

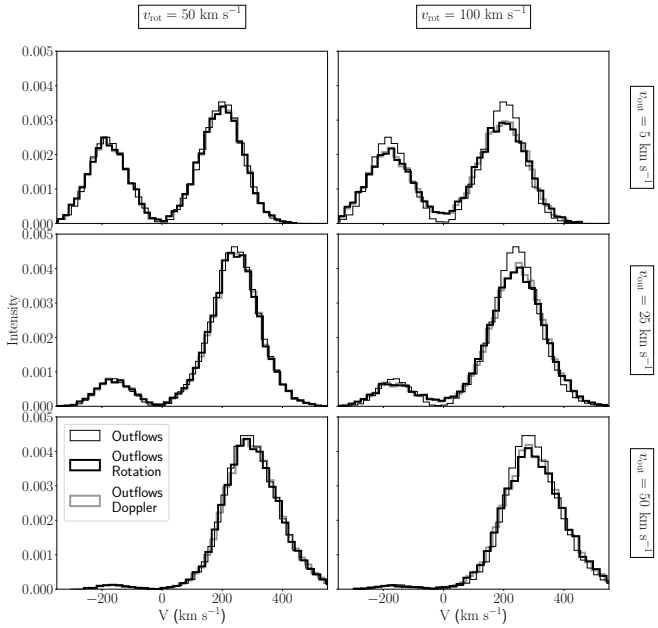

Figure A2. Qualitative trends of changing outflow and rotational velocity. Same layout as Figure 1, this time $\tau_{\rm H} = 10^7$ and $\theta = 90°$.